AGU100 ADVANCING EARTH AND SPACE SCIENCE

Water Resources Research

RESEARCH ARTICLE
10.1029/2018WR023297

Key Points:
- This model incorporates Green-Ampt infiltration concepts into a dynamic multidomain porosity framework
- Model was verified on two soils, improving estimates of infiltration and ponding compared to the classic Green-Ampt model
- Most model parameters can be constrained using universal constants or auxiliary measurements

Correspondence to:
R. D. Stewart,
ryan.stewart@vt.edu

Citation:
Stewart, R. D. (2018). A dynamic multidomain Green-Ampt infiltration model. *Water Resources Research*, *54*. https://doi.org/10.1029/2018WR023297

Received 10 MAY 2018
Accepted 14 AUG 2018
Accepted article online 30 AUG 2018

A Dynamic Multidomain Green-Ampt Infiltration Model

Ryan D. Stewart[1]

[1]School of Plant and Environmental Sciences, Virginia Polytechnic Institute and State University, Blacksburg, VA, USA

Abstract Shrink-swell soils possess dynamic hydraulic properties, which may limit the applicability of traditional models for simulating infiltration and overland flow. This study incorporates Green-Ampt infiltration concepts into a multidomain porosity framework to account for variations in pore size distributions and saturated hydraulic conductivities caused by soil shrinkage and swelling. The model requires three input variables (initial water content, rainfall rate, and time) and up to 15 parameters to simulate infiltration and overland flow, though most of the parameters are universal constants or can be estimated from auxiliary measurements. In comparison, the classic Green-Ampt model, which assumes constant hydraulic properties and a single domain, requires the same three inputs and up to seven parameters to use. Performance of the proposed multidomain model was verified with two data sets. The first came from a study in Mexico where time to ponding and soil matrix infiltration were quantified under simulated rainfall, and the second came from a study in Chile where overland flow was measured during irrigation experiments on runoff plots. By tuning two (Chile) or three (Mexico) parameters, the multidomain model provided accurate estimations of infiltration/runoff partitioning at multiple scales. Compared to the classic single-domain model, the multidomain model had lower root-mean-square deviations (reducing simulated infiltration errors by 2–3 times) and Akaike Information Criterion (AIC) scores (ΔAIC ~100), thus providing better simulations of infiltration, ponding, and runoff. These results demonstrate that modeling hydrological processes in shrink-swell soils necessitates separating soil properties mediated by the matrix from those associated with interblock shrinkage cracks.

Plain Language Summary Many soils develop cracks as they dry. During rainstorms and irrigation events, these cracks permit water to move rapidly, but we do not currently possess appropriate tools to simulate water movement in such conditions. This study proposes a mathematical model that calculates water infiltration into such soils by explicitly accounting for properties of cracks versus those of the surrounding soil. The model was verified using field observations from two locations, which demonstrated that the model can accurately simulate water infiltration, ponding on the soil surface, and surface runoff in soils containing cracks.

1. Introduction

Shrink-swell soils experience dynamic shifts in pore size distributions as crack networks open and close. The resulting variability in soil hydraulic properties has limited the applicability of traditional models to simulate processes such as infiltration, surface runoff (i.e., overland flow), and contaminant transport. For instance, van der Salm et al. (2012) identified shrinkage cracks as the primary conduit by which water and nutrients became transported through a heavy clay soil, yet such preferential flow and transport processes cannot be captured using classic flow and transport models. Recent work has established that multidomain formulations can better simulate water content, hydraulic properties, and solute transport in shrink-swell soils (Coppola et al., 2015; Coppola et al., 2012; Šimůnek et al., 2003; Stewart, Abou Najm, et al., 2016). Still, these approaches have not yet led to satisfactory predictions of water infiltration, ponding, and runoff at the soil surface.

One challenge to modeling infiltration in shrink-swell soils comes from material deformation and subsidence, which causes variations in the thicknesses of individual soil layers. In response, previous efforts have attempted to model water movement through shrink-swell soils using two main approaches: the Lagrangian (material) framework, in which the coordinate dimensions vary along with the soil shrinkage/swelling process, and the Eulerian (physical space) framework, in which the coordinate system remains constant. In the former (Lagrangian) approach, the system coordinates change along with the solid phase, such that the soil surface is typically treated as having a constant position (Davidson, 1984;

Gérard-Marchant et al., 1997). In the latter (Eulerian) approach, soil shrinkage and swelling causes the position of the solid phase to shift relative to the origin of the coordinate system (Bronswijk, 1988; Coppola et al., 2012). Both formulations require descriptions of soil cracks and the soil matrix, either implicitly or else in an explicit multidomain formulation. Water flow can then be described with the Richards equation (Coppola et al., 2012; Lassabatère et al., 2014) or variants thereof (Potkay, 2017), the Green-Ampt model (Davidson, 1984), a water balance approach (Bronswijk, 1988), or the kinematic wave equation (Greco, 2002), often with the restriction that flow only occurs through the shrinkage cracks rather than the soil matrix.

The Green-Ampt model is often used to describe one-dimensional infiltration, as it is easy to use and includes parameters that can be physically constrained. The model also estimates time to ponding, which can be an important parameter for predicting processes such as overland and bypass flow. While most frequently used for single domain, homogenous soils, several studies have applied Green-Ampt concepts within multidomain systems. Davidson (1984) developed a Green-Ampt model in which water could simultaneously infiltrate into a soil matrix from the soil surface (vertical flow) and from regularly distributed soil cracks (horizontal flow), with the stipulation that the distance between cracks is much greater than the width of the cracks. Weiler (2005) incorporated Green-Ampt expressions for vertical and horizontal infiltration to model water exchange and bypass flow in macroporous soils. Neither approach, however, allowed for variations in distributions or properties of the different porosity domains, thus limiting their ability to describe dynamic shrinkage and swelling processes.

Altogether, there exists the need for a simple yet accurate description of infiltration into shrink-swell soils. In response, this study combines the classic Green-Ampt model for one-dimensional vertical infiltration with a dynamic multidomain framework. This approach builds on and expands a multidomain framework previously developed to describe dynamic hydraulic properties (Stewart, Abou Najm, et al., 2016; Stewart, Rupp, et al., 2016), while maintaining the simplicity and ease of use of the Green-Ampt model. This paper is thus constructed to (1) modify the Stewart, Abou Najm, et al. (2016) model to better describe dynamic (transient) saturated hydraulic conductivity of shrink-swell soils and (2) develop and validate an infiltration model for shrink-swell soils that can simulate rainfall partitioning using only estimates for water content, rainfall rate and time, and a minimum of other physically constrained parameters. The model ultimately aims to test the hypothesis that accurately modeling hydrological processes in shrink-swell soils necessitates separating soil properties mediated by the matrix, which may include small-scale interaggregate shrinkage cracks, from those associated with interblock cracks that surround the matrix.

2. Theory

2.1. Porosity Domains

The total porosity (ϕ_{max}) of a shrink-swell soil can be divided into three domains: aggregates (which comprise the soil particles plus any microscale porosity between them), cracks (which represent voids that form as the soil aggregate domain shrinks due to desiccation), and subsidence (which represents a vertical lowering of the soil surface due to soil aggregate shrinkage). As shown by Stewart, Rupp, et al. (2016), the distributions of these domains change as a function of water content, u:

$$\phi_{max} = \phi_{aggr}(u) + \phi_{sub}(u) + \phi_{crack}(u) \tag{1}$$

where the subscripts aggr, crack, and sub refer to the respective aggregate, shrinkage crack, and vertical subsidence domains.

Stewart, Rupp, et al. (2016) then described the porosities of all three domains as

$$\phi_{aggr}(U) = (\phi_{max} - \phi_{min})\left(\frac{p+1}{p+U^{-q}}\right) + \phi_{min} \tag{2}$$

$$\phi_{sub}(U) = \left(1 - (1 - (\phi_{max} - \phi_{min}))^{1/\chi}\right)\left(\frac{1-U^q}{1+pU^q}\right) \tag{3}$$

$$\phi_{crack}(U) = \left((\phi_{max} - \phi_{min}) - 1 + (1 - (\phi_{max} - \phi_{min}))^{1/\chi}\right)\left(\frac{1-U^q}{1+pU^q}\right) \tag{4}$$

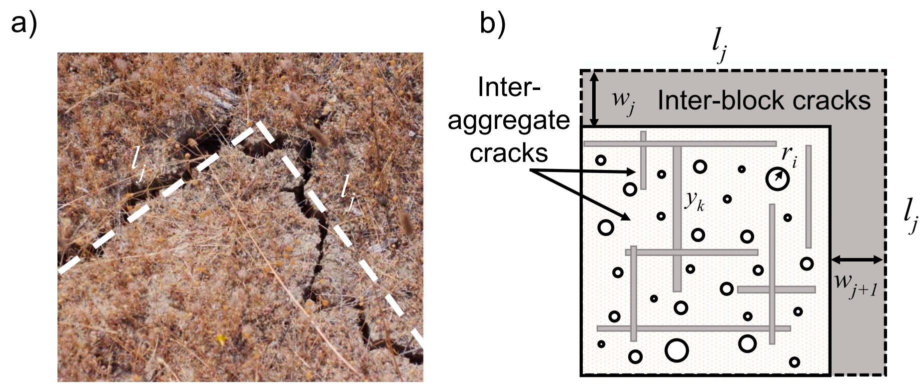

Figure 1. (a) Example of a shrink-swell soil showing visible *border* macrocracks (designated with dashed white lines); (b) theoretical division of the soil porosity into interblock cracks with widths w_j and lengths l_j, interaggregate cracks with widths y_k, and aggregate pores with radii r_i.

where p and q are functional shape parameters, ϕ_{min} is the minimum porosity of the aggregate domain, U is the degree of saturation (determined as water content u divided by its saturated value u_{max}), and χ is the shrinkage geometry factor (Bronswijk, 1990). χ ranges from 1 (pure subsidence) to ∞ (pure cracking), with $\chi = 3$ representing isotropic shrinkage.

Here we further divide the shrinkage crack domain into *internal* interaggregate cracks held within the soil matrix (Chertkov & Ravina, 2002) and *external* interblock cracks that form borders around the soil matrix (Figure 1). In this framework, interaggregate cracks are represented by $\phi_{\text{interaggr}}$, and external cracks are represented by $\phi_{\text{interblock}}$. The two domains are related to the total crack porosity via a proportionality factor Υ ($0 \le \Upsilon \le 1$):

$$\phi_{\text{interblock}}(U) = \Upsilon \phi_{\text{crack}}(U) \tag{5a}$$

$$\phi_{\text{interaggr}}(U) = (1 - \Upsilon)\phi_{\text{crack}}(U) \tag{5b}$$

For purposes of this derivation we will assume Υ is constant, such that the proportion of cracks in the interblock and interaggregate domains are fixed. Note also that in this framework the porosity of the soil matrix $\phi_{\text{matrix}}(U) = \phi_{\text{aggr}}(U) + \phi_{\text{interaggr}}(U)$.

2.2. Multidomain Water Flow

The total flux density of water, J [L T^{-1}], through a cracked soil is

$$J = \frac{Q_{\text{interblock}} + Q_{\text{interaggr}} + Q_{\text{aggr}}}{A_{\text{interblock}} + A_{\text{interaggr}} + A_{\text{aggr}}} = \frac{Q_{\text{interblock}} + Q_{\text{interaggr}} + Q_{\text{aggr}}}{A_{\text{total}}} \tag{6}$$

where Q [L^3 T^{-1}] represents volumetric flow, A [L^2] represents cross-sectional area, with aggr, interaggr, and interbock referring to the respective aggregate, interaggregate crack, and interblock crack domains, and total referring to the combination of all three domains. This expression can be rearranged as

$$J = \left(\frac{A_{\text{interblock}}}{A_{\text{total}}}\right) J_{\text{interblock}} + \left(\frac{A_{\text{interaggr}}}{A_{\text{total}}}\right) J_{\text{interaggr}} + \left(\frac{A_{\text{aggr}}}{A_{\text{total}}}\right) J_{\text{aggr}} \tag{7}$$

We can estimate the ratios of domain areas to total area using the following relationships:

$$\frac{A_{\text{interblock}}}{A_{\text{total}}} = \left(\frac{V_{\text{interblock}}/H_m}{(V_{\text{interblock}} + V_{\text{interaggr}} + V_{\text{aggr}})/H_m}\right) = \left(\frac{\Upsilon \phi_{\text{crack}}(U)}{1 - \phi_{\text{sub}}(U)}\right) \tag{8a}$$

$$\frac{A_{\text{interaggr}}}{A_{\text{total}}} = \left(\frac{V_{\text{interaggr}}/H_m}{(V_{\text{interblock}} + V_{\text{interaggr}} + V_{\text{aggr}})/H_m}\right) = \left(\frac{(1 - \Upsilon)\phi_{\text{crack}}(U)}{1 - \phi_{\text{sub}}(U)}\right) \tag{8b}$$

$$\frac{A_{\text{aggr}}}{A_{\text{total}}} = \left(\frac{V_{\text{aggr}}/H_m}{\left(V_{\text{interblock}} + V_{\text{interaggr}} + V_{\text{aggr}}\right)/H_m} \right) = \left(\frac{1 - \phi_{\text{crack}}(U) - \phi_{\text{sub}}(U)}{1 - \phi_{\text{sub}}(U)} \right) \tag{8c}$$

where H_m [L] is the height of the soil matrix and V [L^3] represents the volumes of the various domains. Substituting equation (8a) into equation (7)

$$J = \left(\frac{\Upsilon \phi_{\text{crack}}(U)}{1 - \phi_{\text{sub}}(U)} \right) J_{\text{interblock}} + \left(\frac{(1-\Upsilon)\phi_{\text{crack}}(U)}{1 - \phi_{\text{sub}}(U)} \right) J_{\text{interaggr}} + \left(1 - \frac{\phi_{\text{crack}}(U)}{1 - \phi_{\text{sub}}(U)} \right) J_{\text{aggr}} \tag{9}$$

Darcy's law, which states that $J = K\nabla\Psi$ (where K [L T^{-1}] represents hydraulic conductivity and $\nabla\Psi$ [L L^{-1}] the hydraulic gradient driving water movement), can be applied to equation (9):

$$\begin{aligned} K\nabla\Psi = &\left(\frac{\Upsilon \phi_{\text{crack}}(U)}{1 - \phi_{\text{sub}}(U)} \right) K_{\text{interblock}} \nabla\Psi_{\text{border}} \\ &+ \left[\left(\frac{(1-\Upsilon)\phi_{\text{crack}}(U)}{1 - \phi_{\text{sub}}(U)} \right) K_{\text{interaggr}} + \left(1 - \frac{\phi_{\text{crack}}(U)}{1 - \phi_{\text{sub}}(U)} \right) K_{\text{aggr}} \right] \nabla\Psi_{\text{matrix}} \end{aligned} \tag{10}$$

Note that equation (10) assumes that the hydraulic gradients for the interaggregate cracks and the soil aggregates are equivalent and can be represented by a single value $\nabla\Psi_{\text{matrix}}$, while the hydraulic gradient through the interblock cracks is represented by a distinct gradient $\nabla\Psi_{\text{border}}$.

2.3. Multidomain Hydraulic Conductivities

While equation (10) can be used assuming constant hydraulic conductivity values for the different pore domains, in many clay soils the shrinkage and swelling processes cause pore deformations that may alter soil permeability. In this section it will be assumed that the aggregate domain has its maximum hydraulic conductivity when the soil is saturated ($U = 1$), whereas the interaggregate and interblock crack domains will have maximum hydraulic conductivities when the soil is dry ($U = 0$).

An earlier derivation for multidomain dynamic hydraulic conductivity (Stewart, Abou Najm, et al., 2016) considered two geometric models for shrinkage cracks. In the first, shrinkage consisted solely of larger cracks that dissected the soil into discrete islands (i.e., border cracks), while in the second, shrinkage occurred in cracks distributed within the soil matrix. For interblock border cracks, the width of a crack w_j [L] scales to its the maximum width $w_{j,\max}$ [L] via the relationship first derived in equation (23) of Stewart, Abou Najm, et al. (2016):

$$w_j = w_{j,\max} \left(\frac{1 - U^q}{1 + pU^q} \right) \tag{11}$$

For interaggregate cracks, the width of a crack y_k [L] scales to its maximum width $y_{k,\max}$ [L] via the relationship derived in equation (A3b) of Stewart, Abou Najm, et al. (2016):

$$y_k = y_{k,\max} \left(\frac{1 - U^q}{1 + pU^q} \right)^{1/2} \tag{12}$$

We can then use the Poiseuille equation and assume characteristic geometries (e.g., cylindrical pores for the aggregates and platy pores that resemble parallel plates for the cracks) to derive expressions for the *transient* saturated hydraulic conductivity of these porosity domains as functions of water content. Starting with the interblock cracks that exist external to the soil matrix, we can solve for their transient saturated hydraulic conductivity ($K_{\text{interblock}}$) as

$$K_{\text{interblock}}(U) = \sum_{j=1}^{N} \frac{l_j \rho_f g w_j^3}{12 \mu_f A_{\text{interblock}} \tau_j^2} = K_{\text{interblock},\max} \left(\frac{1 - U^q}{1 + pU^q} \right)^2 \tag{11}$$

where l_j [L] is the length and τ_j [L L^{-1}] is the tortuosity of crack j, ρ_f [M L^{-3}] is the density of the fluid (water), g [L T^{-2}] is the gravitational acceleration, μ_f [M L^{-1} T^{-1}] is the fluid viscosity, and $K_{\text{interblock,max}}$ [L T^{-1}] is the maximum hydraulic conductivity of the interblock crack domain (when $U = 0$). An expression similar to equation (11) was first derived in equation (25) of Stewart, Abou Najm, et al. (2016).

We can use a similar approach for the interaggregate cracks distributed within the soil matrix and determine their transient saturated hydraulic conductivity, $K_{\text{interaggr}}$ [L T^{-1}], as

$$K_{\text{interaggr}}(U) = \sum_{k=1}^{O} \frac{A_k \rho_f g {y_k}^2}{12 \mu_f A_{\text{interaggr}} {\tau_k}^2} = K_{\text{interaggr, max}} \left(\frac{1-U^q}{1+pU^q} \right) \tag{12}$$

where A_k [L^2] is the cross-sectional area of crack k, τ_k [L L^{-1}] is a tortuosity factor for interaggregate cracks, and $K_{\text{interaggr,max}}$ [L T^{-1}] is the maximum hydraulic conductivity of the interaggregate crack domain (when $U = 0$). A similar result to equation (12) was first derived in equations (A4) and (A5) of Stewart, Abou Najm, et al. (2016).

Finally, we can analyze the transient saturated hydraulic conductivity of the aggregates within the soil matrix, K_{aggr} [L T^{-1}], using equations (30) and (31) of Stewart, Abou Najm, et al. (2016):

$$K_{\text{aggr}}(U) = K_{\text{aggr, max}} \left(\frac{p+1}{p+U^{-q}} \right) + K_{\text{aggr, min}} \left(\frac{1-U^q}{1+pU^q} \right) \tag{13a}$$

$$K_{\text{aggr, min}} = \sum_{i=1}^{M} \frac{\pi {r_{i,\text{max}}}^2 \rho_f g}{8 \mu_f A_t {\tau_i}^2} {r_{i,\text{min}}}^2 \tag{13b}$$

$$K_{\text{aggr, max}} = \sum_{i=1}^{M} \frac{\pi {r_{i,\text{max}}}^2 \rho_f g}{8 \mu_f A_t {\tau_i}^2} {r_{i,\text{max}}}^2 \tag{13c}$$

where τ_i is the tortuosity factor for pore i [L L^{-1}] and A_i is the area of pore I [L^2]. The original derivation assumed that the minimum hydraulic conductivity of the aggregate domain ($K_{\text{aggr,min}}$) could be considered negligible. Here we revise that assumption and express the ratio of minimum and maximum transient hydraulic conductivities as

$$\frac{K_{\text{aggr, min}}}{K_{\text{aggr, max}}} = \sum_{i=1}^{M} {r_{i,\text{min}}}^2 \Big/ \sum_{i=1}^{M} {r_{i,\text{max}}}^2 \cong \frac{\phi_{\text{min}}}{\phi_{\text{max}}} \tag{14}$$

Putting these expressions together, we define the area-weighted transient saturated hydraulic conductivity of the soil matrix (K_{matrix}) and the surrounding border cracks (K_{border}) as

$$\begin{aligned} K_{\text{matrix}}(U) = {} & K_{\text{interaggr, max}} \left(\frac{(1-\Upsilon)\phi_{\text{crack}}(U)}{1-\phi_{\text{sub}}(U)} \right) \left(\frac{1-U^q}{1+pU^q} \right) + \\ & K_{\text{aggr, max}} \left(1 - \frac{\phi_{\text{crack}}(U)}{1-\phi_{\text{sub}}(U)} \right) \left[\left(\frac{p+1}{p+U^{-q}} \right) + \left(\frac{\phi_{\text{min}}}{\phi_{\text{max}}} \right) \left(\frac{1-U^q}{1+pU^q} \right) \right] \end{aligned} \tag{15}$$

$$K_{\text{border}}(U) = K_{\text{interblock, max}} \left(\frac{\Upsilon \phi_{\text{crack}}(U)}{1-\phi_{\text{sub}}(U)} \right) \left(\frac{1-U^q}{1+pU^q} \right)^2 \tag{16}$$

2.4. Green-Ampt Model

The Green-Ampt infiltration model simulates one-dimensional vertical infiltration assuming a sharp wetting front and that the capillary force is described as a wetting front potential, h_f [L]. In the case of a negligible surface ponding depth, the hydraulic gradient can be approximated as $\nabla\Psi = (h_f + z)/z$, where z is the depth of the wetting front beneath the soil surface. The wetting front depth can be estimated from the cumulative depth of infiltrated water, I [L], as $z = I/n_e$, where n_e is the available pore space. The n_e can be calculated in terms of initial volumetric water content θ_i or initial degree of saturation U_i as

$$n_e = \theta_s - \theta_i = \phi_{\text{max}}(1-U_i) \tag{17}$$

This expression allows the hydraulic gradient to be written as $\nabla\Psi = 1 + h_f n_e / I$.

To apply the Green-Ampt model in a multidomain formulation, we first must divide the rainfall between the soil matrix and border crack domains. For initial times, when both domains absorb the rainfall, we can partition the area-weighted rainfall between domains r_{matrix} and r_{border} (using the relative areas described with equation (8a)) as

$$r_{\text{matrix}}(U) = \left(\frac{A_{\text{interaggr}} + A_{\text{aggr}}}{A_{\text{total}}}\right) r = \left(1 - \frac{\Upsilon \phi_{\text{crack}}(U)}{1 - \phi_{\text{sub}}(U)}\right) r \qquad t \leq t_{p,\text{matrix}} \tag{18a}$$

$$r_{\text{border}}(U) = \left(\frac{A_{\text{interblock}}}{A_{\text{total}}}\right) r = \left(\frac{\Upsilon \phi_{\text{crack}}(U)}{1 - \phi_{\text{sub}}(U)}\right) r \qquad t \leq t_{p,\text{matrix}} \tag{18b}$$

where $t_{p,\text{matrix}}$ is the time of ponding in the soil matrix. Ponding on the soil matrix occurs when the rainfall rate equals the infiltration rate into the matrix, i_{matrix}. Here we use the Green-Ampt approximation first derived in equation (5) of Selker and Assouline (2017):

$$i_{\text{matrix}} = K_{\text{matrix}}(U) + \frac{AK_{\text{matrix}}(U) + \sqrt{\frac{n_e K_{\text{matrix}}(U) h_{f,\text{matrix}}}{2t}}}{1 + A\frac{K_{\text{matrix}}(U)t}{n_e h_{f,\text{matrix}}} + \sqrt{\frac{2K_{\text{matrix}}(U)t}{n_e h_{f,\text{matrix}}}}} \tag{19}$$

where A is a constant typically taken to equal 2/3.

The time to matrix ponding ($t_{p,\text{matrix}}$) can be determined by finding the time when the matrix infiltration rate equals the rainfall rate. Substituting $r_{\text{matrix}}(U)$ into equation (19) and rearranging allows us to implicitly determine $t_{p,\text{matrix}}$ as

$$r_{\text{matrix}}(U)/K_{\text{matrix}}(U) = 1 + \frac{A + \sqrt{\frac{n_e h_{f,\text{matrix}}}{2K_{\text{matrix}}(U)t_{p,\text{matrix}}}}}{1 + A\frac{K_{\text{matrix}}(U)t_{p,\text{matrix}}}{n_e h_{f,\text{matrix}}} + \sqrt{\frac{2K_{\text{matrix}}(U)t_{p,\text{matrix}}}{n_e h_{f,\text{matrix}}}}} \tag{20}$$

The cumulative infiltration into the soil matrix, I_{matrix} [L], can be expressed as

$$I_{\text{matrix}} = r_{\text{matrix}}(U)t \qquad t \leq t_{p,\text{matrix}} \tag{21a}$$

$$I_{\text{matrix}} = r_{\text{matrix}}(U)t_{p,\text{matrix}} + \int_{t_{p,\text{matrix}}}^{t} i_{\text{matrix}} dt' \qquad t > t_{p,\text{matrix}} \tag{21b}$$

where t' is a dummy variable of integration.

After integrating equation (21b), I_{matrix} is written as

$$I_{\text{matrix}} = r_{\text{matrix}}(U)t \qquad t \leq t_{p,\text{matrix}} \tag{22a}$$

$$I_{\text{matrix}} = r_{\text{matrix}}(U)t_{p,\text{matrix}} + K_{\text{matrix}}(U)\left(t - t_{p,\text{matrix}}\right) + n_e h_{f,\text{matrix}} \ln\left[\frac{1 + A\frac{K_{\text{matrix}}(U)t}{n_e h_{f,\text{matrix}}} + \sqrt{\frac{2K_{\text{matrix}}(U)t}{n_e h_{f,\text{matrix}}}}}{1 + A\frac{K_{matrix}(U)t_{p,\text{matrix}}}{n_e h_{f,\text{matrix}}} + \sqrt{\frac{2K_{\text{matrix}}(U)t_{p,\text{matrix}}}{n_e h_{f,\text{matrix}}}}}\right] \qquad t > t_{p,\text{matrix}} \tag{22b}$$

We now turn to the border domain and make the assumption that interblock cracks have sufficient width to render the capillary force negligible (i.e., the wetting front potential $h_f \approx 0$ in cracks). This assumption means that water will flow through the cracks under a unit hydraulic gradient, that is, $\nabla\Psi_{\text{border}} = 1$. We also assume that once ponding on the soil matrix commences, excess water will be delivered into these border cracks.

The infiltration rate into the interblock crack (border) domain, i_{border} [L T^{-1}], can be expressed as

$$i_{\text{border}} = \min(r_{\text{border}}(U), K_{\text{border}}(U)) \qquad t \leq t_{p,\text{matrix}} \tag{23a}$$

$$i_{\text{border}} = \min(r - i_{\text{matrix}}, K_{\text{border}}(U)) \qquad t > t_{p,\text{matrix}} \tag{23b}$$

As an additional constraint, cracks often have finite storage volumes. If we define the effective crack depth D_{border} as being equal to the interblock crack domain volume divided by the mean domain cross-sectional area, the cumulative infiltration into the border domain (I_{border}) can then be defined as

$$I_{\text{border}} = \min(r_{\text{border}}(U)t, K_{\text{border}}(U)t, D_{\text{border}}) \qquad t \le t_{p,\text{matrix}} \tag{24a}$$

$$I_{\text{border}} = \min\left(r_{\text{border}}(U)t_{p,\text{matrix}} + r\left(t - t_{p,\text{matrix}}\right) - \left(I_{\text{matrix}} - I_{p,\text{matrix}}\right), K_{\text{border}}(U)t, D_{\text{border}}\right) \qquad t > t_{p,\text{matrix}} \tag{24b}$$

Note that for simplicity we did not explicitly consider losses from the crack into the matrix due to horizontal infiltration, though the D_{border} term could be modified to incorporate such processes, for example, with a horizontal G&A model (Novák et al., 2000; Stewart et al., 2014; Weiler, 2005).

Finally, the total infiltration into the soil matrix, I [L], can be determined as

$$I = I_{\text{matrix}} + I_{\text{border}} \tag{25}$$

and the total depth of overland flow, OF [L], can be quantified as

$$OF = rt - s - I \tag{26}$$

where s represents any surface storage, for example, in shallow depressions.

2.5. Soil Water Content

The model will work with either measured or modeled water content as input. To model the water content, an initial estimate of U_i is needed. From there, assuming that the infiltrated water is stored in the soil over some depth D_{soil} (defined as being positive upward to the surface), the change in water content in the soil can be modeled as

$$\Delta U = I/(u_{\max} D_{\text{soil}}) \tag{27}$$

3. Field Data for Model Verification

To test the hypothesis that a dynamic multidomain formulation better simulates infiltration and overland flow in shrink-swell soils, results from the above multidomain model were compared with a classic single-domain Green-Ampt formulation (i.e., using equation (22a) and only considering a single soil domain with $K_{\text{matrix}} = K_{\text{aggr,max}}$). Observational data for model verification came from two field sites: one in northeastern Mexico (Návar et al., 2002) and the other from south central Chile (Stewart et al., 2015).

The full form of the multidomain model requires the following parameters (with definitions listed in the Notation section): A (typically assumed to be 2/3); s [L]; $h_{f,\text{matrix}}$ [L]; D_{soil} [L]; $u_{\max}$ [M M^{-1}]; $K_{\text{aggr,max}}$ [L T^{-1}]; $\phi_{\max}$ [L^3 L^{-3}]; D_{border} [L]; $\phi_{\min}$ [L^3 L^{-3}]; $K_{\text{interblock,max}}$ [L T^{-1}]; $K_{\text{interaggr,max}}$ [L T^{-1}]; Υ $(0 \le \Upsilon \le 1)$ [−]; χ $(\chi \ge 1)$ [−]; p [−]; and q [−]. Note that the first seven terms were also required for the single-domain Green-Ampt model. Both models also require estimates for rainfall rate, r [L T^{-1}], and initial degree of saturation, U_i.

The following subsections list a brief overview of the experimental setups and the methods by which the above parameters were either constrained (using reported and assumed values) or retained as fitting parameters.

3.1. Mexico Site

The first data set used to verify the multidomain model came from Návar et al. (2002). In that study, simulated rainfall was applied to a shrink-swell soil located in northeastern Mexico. Crack width, time to ponding, and water velocity and discharge into discrete cracks were measured during the experiments. Surface runoff did not propagate down the hillslope, as the cracks did not fully close during the rainfall experiments. Tensiometers measured matric potential at 100-, 200-, and 300-mm depths, and soil samples were used to estimate gravimetric water contents throughout the study. Note that the original study reported data from two 11.3-m × 1.3-m runoff plots, whereas the analysis here combines the individual plot data

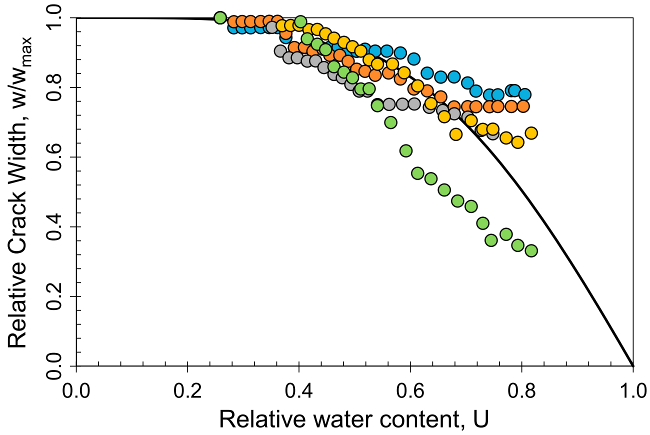

Figure 2. Relative crack width, w/w_{max}, versus degree of saturation, $U = u/u_{max}$, for five measured cracks in the Mexico site (points). The line represents modeled crack width using equation (11) and values of p = 0.5 and q = 4.15.

into mean values for precipitation duration and intensity, time to ponding, and infiltration depths into the matrix versus cracks.

To parameterize the multidomain infiltration model, values of D_{soil} = 800 mm and ϕ_{max} = 0.525 m^3/m^3 were taken as reported in the original study. u_{max} was constrained by assuming a solid particle density of 2.65 Mg/m^3 and using the relationship $u_{max} = \frac{\rho_w}{\rho_s}\left(\frac{\varphi_{max}}{1-\varphi_{max}}\right)$, which resulted in an estimated value of 0.417 g/g. The soil characteristic curve (i.e., gravimetric water content versus soil matric potential) was estimated by fitting the van Genuchten (1980) model to the saturated water content and three other reported gravimetric water content/matric potential data points, using a least squares regression. This curve allowed for conversion between the reported matric potential values and the equivalent gravimetric water content values (u), which are required to interpret soil shrinkage characteristics using the framework developed here. The retention data were generated during a wetting experiment and therefore are assumed to represent the primary wetting curve.

Soil shrinkage parameters were determined by analyzing changes in interblock widths as recorded in the rainfall experiment and then applying the relative crack width model from equation (11). The p and q were fit by minimizing the root-mean-square deviation (RMSD) between measured and modeled crack widths, which resulted in values of p = 0.5 and q = 4.15 (Figure 2).

The crack porosity distribution factor Υ was constrained as 0.75; a brief sensitivity analysis showed negligible sensitivity to this parameter so long as $K_{interaggr,max}$ and $K_{aggr,max}$ were left unconstrained. Isotopic shrinkage (χ = 3) was assumed. ϕ_{min} was set to 0.325 m^3/m^3 to match the observed maximum (interblock) crack porosity of 0.10 m^3/m^3 (as calculated using equation (5a)).

With the aforementioned parameters, the matrix infiltration was modeled using equations (19)–(22a). The h_f, $K_{interaggr,max}$, and $K_{aggr,max}$ were constrained using least squares regression between the measured and modeled cumulative infiltration (I_{matrix}) and time to ponding on the soil matrix ($t_{p,matrix}$). Three simulated rainfall events occurred with spacing of 1 and then 4 days; the measured initial water on the first day of the experiment was used to set U_i in the model. U_i values for subsequent rainfall events were estimated using equation (27).

3.2. Chile Site

The second data set came from a study conducted by Stewart et al. (2015). The experimental site was located near Ninhue, Chile (36°25′04″S, 72°31′05″W), on a hillslope vegetated with unmaintained and ungrazed pasture. Eighteen 3.5 × 11-m plots were placed in two clusters (referred to as *Upper* and *Lower* plots), and in each cluster were numbered from 1 to 9, for example, L1, U1. In 2012, 12 of the plots received simulated rainfall from an irrigation system, with three plots receiving water simultaneously (i.e., L1-L3, L4-L6, U1-U3, and U4-U6). Each irrigation event lasted 52–115 min, with rainfall rates between 0.28 and 0.84 mm/min (as measured using distributed catch cans). Each plot received four to six discrete irrigation events over a 3-week period, with cumulative applied irrigation of 185–355 mm. Plot instrumentation and data collection are further detailed in Stewart et al. (2015).

Soil water content sensors (Decagon Devices 5TM, Pullman, WA) were installed at four depths (150, 300, 600, and 850 mm) in Plots L2-L5, U2-U4, and U6, and at two depths (150 and 300 mm) in Plots L1, L6, U1, and U5. Volumetric soil samples (50-mm diameter by 50-mm height) were collected from the plots prior to and after irrigation events to verify measured water content values and estimate bulk density of the soil matrix. Twenty-eight of those cores, collected between 50- and 850-mm depths, were also analyzed in the laboratory for water retention using a positive pressure system. The van Genuchten (1980) retention model was fit to each sample using a least squares regression, and the mean α and n parameter values were then used in equation (15) from Morel-Seytoux et al. (1996) to calculate wetting front potential. This analysis provided a mean value of h_f = 300 mm.

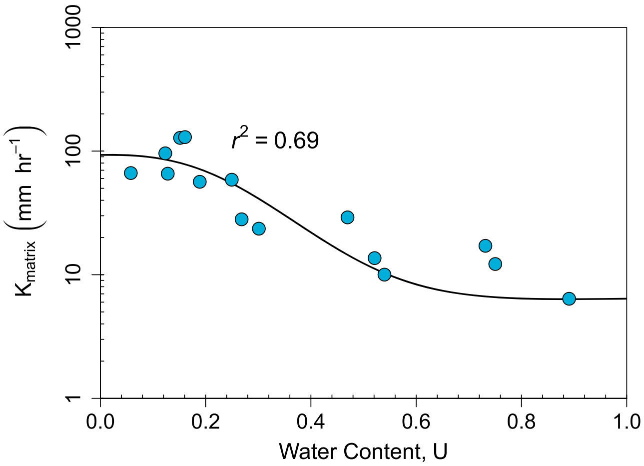

Figure 3. Measured K_{matrix} values in the Chile site based on single-ring infiltration tests (points represent the geometric mean of 5–10 individual tests performed at a given initial degree of saturation *U*). The solid black line represents the *best fit* for equation (15).

Soil shrinkage parameters were determined using shrinkage measurements on peds collected from the site (Stewart, Rupp, et al., 2016), giving values of p = 13.0 and q = 2.76. $K_{interaggr,max}$ and $K_{aggr,max}$ were determined from repeated single-ring infiltration tests performed in the plots throughout the irrigation experiments, following the procedure of Stewart, Abou Najm, et al. (2016). The following modifications were made here: (1) the observed transient saturated hydraulic conductivities were calculated using equations (3) and (12) from Stewart and Abou Najm (2018) assuming a capillary length of 30 cm; (2) the measured hydraulic conductivity values were assumed to represent K_{matrix}, such that equation (15) was fit to the measured values using least squares regression; (3) the crack porosity distribution factor Υ was again set as 0.75; and (4) $K_{aggr,max}$ was set equal to the minimum measured hydraulic conductivity (based on the geometric mean of nine tests performed at an initial water content U_i = 0.89). This analysis resulted in estimated values of $K_{interaggr,max}$ = 33.2 mm/min and $K_{aggr,max}$ = 0.107 mm/min (Figure 3). Note that because the infiltration tests were collected within the soil matrix, $K_{interaggr,max}$ was deemed a more appropriate parameter than $K_{interblock,max}$ (which instead represents the border cracks that were present when the soil was dry).

Initial water contents (U_i) were set based on the mean volumetric water content values from the installed soil moisture sensors (150 and 300 mm or 150, 300, 600, and 850 mm), with plots L5, L6, U3, U4, and U6 set as U_i = 0.5 due to nonfunctioning sensors or high initial water content readings in those plots. Overland flow (runoff) was estimated from equation (26) using the total modeled infiltration from equation (25). Specific storage (s) was assumed to be negligible. D_{soil} was set to either 1,000 or 1,400 mm, depending on which value best matched the observed runoff response. $K_{interblock,max}$ was treated as a universal fitting parameter and was constrained via least squares optimization between measured and modeled cumulative runoff for all plots.

Finally, crack volumes were measured in five discrete cracks (two in Plot L1, two in Plot L4, and one in Plot U3) using a displacement-based sensor (Stewart et al., 2012). These volumes were compared to interblock crack porosities ($\phi_{interblock}$) modeled by combining equations (4) and (5a). To ensure consistent comparison, all volumes/porosities were normalized to the maximum value observed or modeled for each plot or crack (e.g., $\phi_{interblock}/\phi_{interblock,max}$, where $\phi_{interblock,max}$ represents the initial crack porosity).

3.3. Model Evaluation

For the Mexico site, modeled time to ponding and infiltration into the soil matrix were compared. For the Chile site, modeled (OF) versus measured (ÔF) amounts of overland flow were analyzed on both per event and cumulative bases. Specific comparison metrics include R^2 and slope of the regression lines, and RMSD.

RMSD was determined, using overland flow as an example, with

$$RMSD = \sqrt{\frac{\sum_{b=1}^{n}\left(\widehat{OF}_j - OF_j\right)^2}{n}} \tag{27}$$

where n is the number of observations.

Cumulative overland flow data from the Chile site were also analyzed using the Akaike Information Criterion (AIC). With the assumption of normally distributed errors and neglecting an unknown additive constant, AIC was estimated as

$$AIC = n\ln\left(\frac{1}{n}\sum_{b=1}^{n}\left(\widehat{OF}_j - OF_j\right)^2\right) + 2Z \tag{28}$$

where Z is the number of parameters in each model formulation. Because s and D_{border} were not included in this analysis, the multidomain model used 13 parameters versus 6 for the single-domain model.

10.1029/2018WR023297

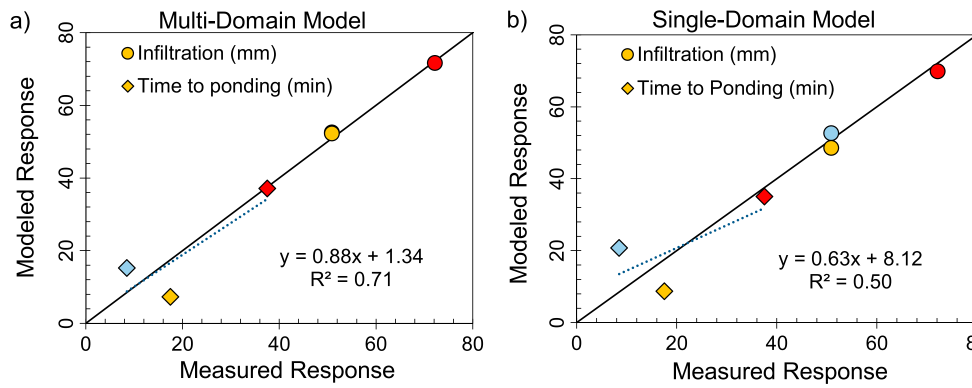

Figure 4. Measured versus modeled infiltration (mm) and time to ponding (min) during a rainfall simulation experiment in the Mexico site. The modeled data come from (a) the proposed multidomain Green-Ampt model versus (b) the traditional single-domain Green-Ampt model. The red color represents the first simulated rainstorm, the blue color represents the second simulated rainstorm, and the yellow color represents the third simulated rainstorm. The trendline represents the time of ponding data.

4. Results

4.1. Mexico Site

The two models (i.e., the proposed multidomain Green-Ampt model and the traditional single-domain Green-Ampt model) were used to simulate matrix infiltration and ponding caused by a rainfall experiment conducted in northeastern Mexico (Figure 4). For the multidomain model, calibration via least squares optimization gave parameter values of $h_{f,\mathrm{matrix}}$ = 67.1 mm, $K_{\mathrm{interaggr,max}}$ = 11.1 mm/min, and $K_{\mathrm{aggr,max}}$ = 0.794 mm/min. The calibrated single-domain model had parameter values of h_f = 164 mm and K_{matrix} = 0.564 mm/min. The multidomain model simulated time to ponding with an overall RMSD of 4.1 min compared to observations, and a total amount of infiltration that varied from observed with an RMSD of 0.71 mm. The single-domain model had greater error in time to ponding (RMSD = 5.1 min) and infiltration (RMSD = 1.3 mm). As a result, the multidomain model reduced RMSD for infiltration by nearly a factor of 2 compared to the single-domain model, with the biggest improvement seen in the first simulated rainstorm (the red points in Figure 4), when the soil profile was initially dry. The multidomain model regression line (fit between measured and modeled time of ponding) had a higher R^2 value than the single-domain model regression line (0.71 for the multidomain model; 0.50 for the single-domain model), with a slope of 0.88 for the multidomain model regression versus 0.63 for the single-domain model regression.

4.2. Chile Site

Overland flow amounts for 12 runoff plots installed in Chile were also modeled using the multidomain Green-Ampt model and the traditional single-domain version. When using a global calibrated value of $K_{\mathrm{interblock,max}}$ = 4,860 mm/min and D_{soil} values of either 1,000 or 1,400 mm, the multidomain model simulated runoff values that closely matched observations (Figures 5a–5c). The model provided better fits to the cumulative runoff (i.e., runoff across all irrigation events) compared to the per event simulations, with R^2 = 0.95 for the modeled versus observed cumulative runoff versus R^2 = 0.84 for the per event values. Both regression lines had slopes near 1 (0.98 for the cumulative runoff; 0.99 for the per event runoff). The AIC score based on the cumulative runoff information was 435, and the RMSD for the modeled versus observed cumulative runoff from all plots was 4.6 mm. The model also modeled soil water content values accurately, with R^2 value between measured and modeled water content of 0.79, and a regression line slope of 0.76.

When using a global calibrated K_{matrix} value of 0.226 mm/min, the simulations from the single-domain Green-Ampt model were relatively poor in terms of per event and cumulative surface runoff (Figures 5d–5f). For the cumulative runoff, the model had an R^2 of 0.66, an RMS deviation of 12 mm, and an AIC score of 529. The per event simulations had an R^2 score of 0.44 compared to

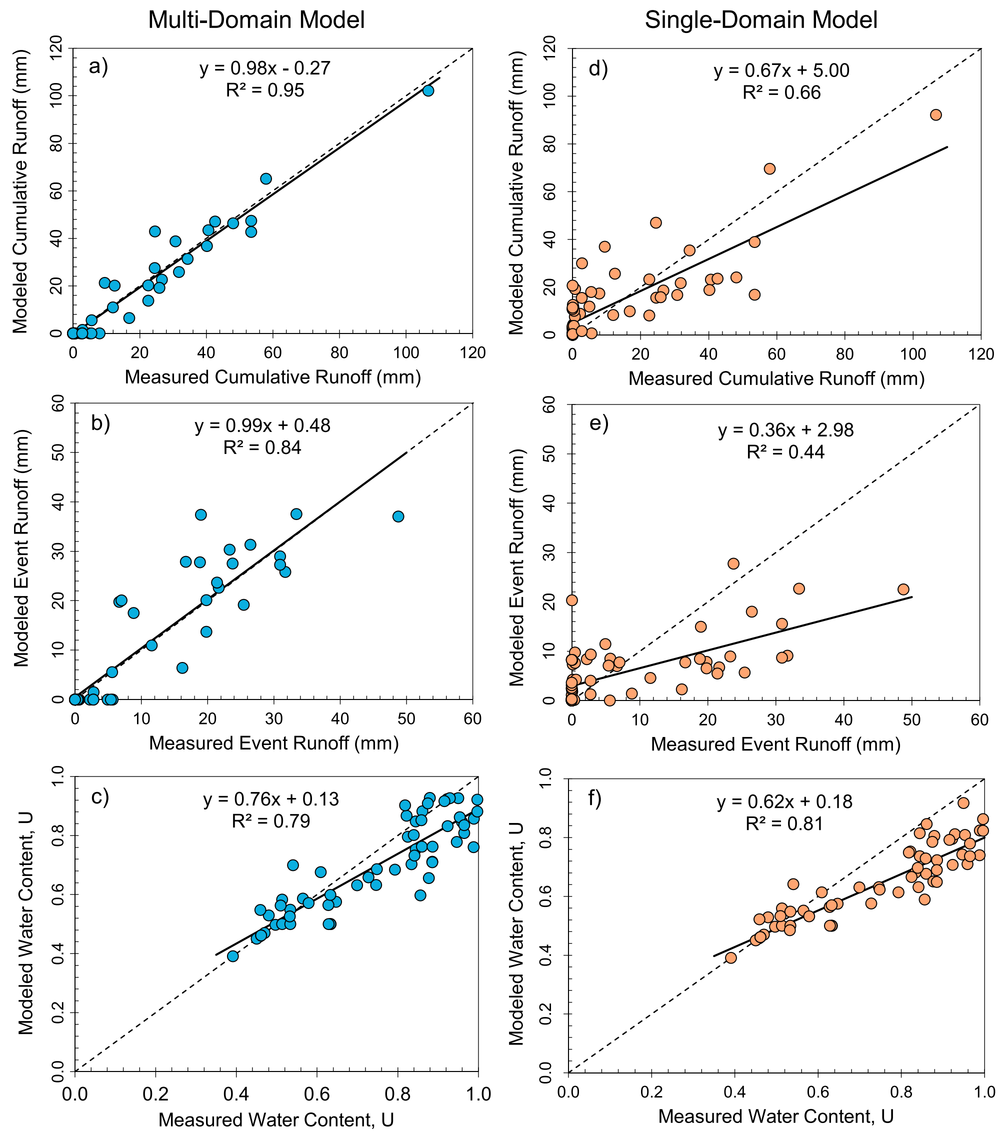

Figure 5. Measured versus modeled surface runoff (i.e., overland flow) for the 12 Chile plots, showing cumulative (a and b) and per event runoff (d and e), along with measured versus modeled soil water content, *U* (c and f). Data in (a)–(c) come from the proposed dynamic multidomain Green-Ampt model, and in (d)–(f) from the traditional single-domain Green-Ampt model. The solid lines show the linear trends; the dashed lines show a 1:1 relationship.

observations. Both regression lines had slopes less than 1 (0.67 for the cumulative runoff and 0.36 for the per event runoff). The modeled versus measured soil water content had a R^2 value of 0.81, with a regression line slope of 0.62.

Both models were also examined for their ability to simulate runoff as a function of cumulative rainfall (note that Figure 6 shows a subset representing the plots with the most cumulative runoff: L1, L5, and U4). In all cases, the multidomain dynamic model better represented the amounts of rainfall required to initiate overland flow (Figure 7), varying from the observed thresholds by ≤30 mm. The single-domain model mostly underestimated the amount of rainfall needed for surface runoff to begin by as much as 130 mm. The superior performance of the multidomain model was also reflected in Nash-Sutcliffe Efficiency (NSE) values: the multidomain model had NSE values greater than 0.9 for 9 of the 12 plots, whereas the single-domain model NSE never reached that threshold.

Finally, the interblock crack widths modeled by the multidomain model were compared to crack widths measurements for discrete cracks during the experiments. In relative terms, the modeled crack porosity

10.1029/2018WR023297

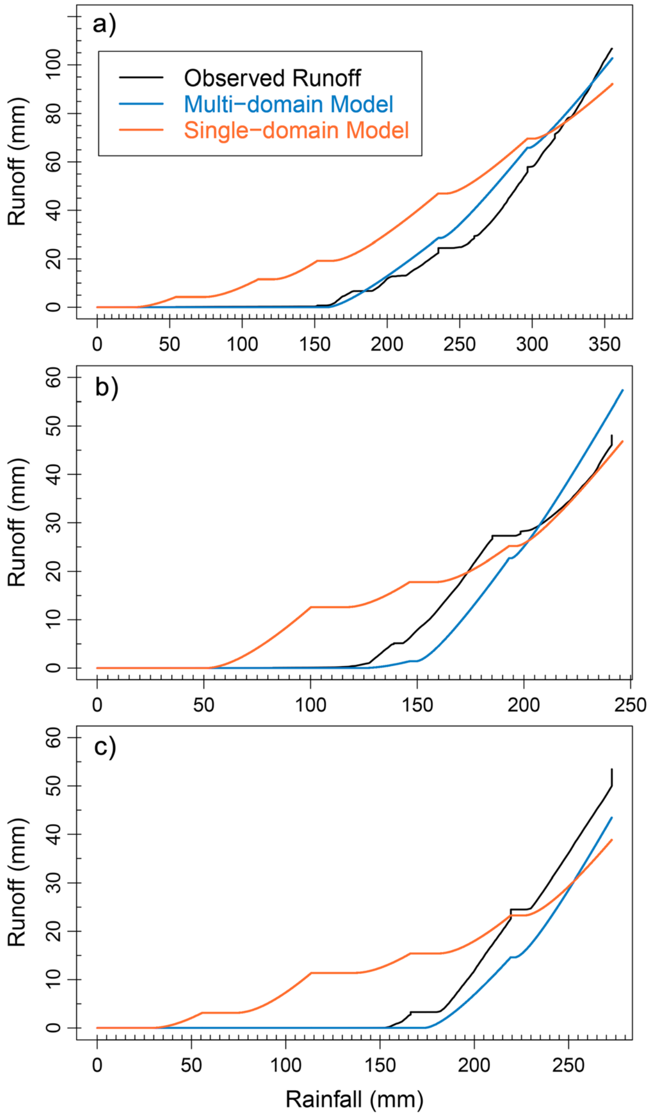

Figure 6. Cumulative runoff (i.e., overland flow) versus cumulative rainfall measured in Chile plots (a) L1, (b) L5, and (c) U4. The black lines represent observed values, blue lines represent the multidomain model, and orange lines represent the single-domain Green-Ampt model.

($\phi_{\text{interblock}}/\phi_{\text{interblock,max}}$) matched closely with the measured crack width ($w_j/w_{j,\text{max}}$), with a regression line R^2 of 0.87 and slope of 0.92 (Figure 8).

5. Discussion and Conclusions

The model developed in this study combined a multidomain framework for simulating dynamic shifts in porosity distributions and hydraulic properties with Green-Ampt infiltration concepts and assumptions (e.g., sharp wetting front and soil capillary force represented by a *wetting front potential*). The resulting multidomain model can simulate the partitioning of water between adsorption into the soil matrix versus bypass flow into soil cracks, as well as initiation of overland flow when that capacity is exceeded. The model was verified using data from two studies at distinct scales: a study in Mexico that examined infiltration and ponding within individual soil matrix blocks, versus a study in Chile that quantified thresholds and magnitudes of overland flow generation at the plot scale.

By every metric tested, the performance of the multidomain model exceeded that of the traditional single-domain Green-Ampt model, thus supporting the hypothesis that modeling hydrological processes in shrink-swell soils necessitates separating soil matrix properties from those properties mediated by interblock cracks. For instance, the *best fit* single-domain model tended to underestimate the amount of rainfall required to initiate matrix ponding (the Mexico site) and overland flow (the Chile site), while also underestimating runoff ratios for high antecedent moisture conditions (Figure 6). The multidomain model, in contrast, more closely approximated times to ponding (Figures 4 and 7) and magnitudes of infiltration/overland flow (Figures 4 and 5), while also reflecting variability in runoff ratios that occurred depending on the size and connectivity of crack networks. Differences in model accuracies were reflected in the AIC scores, where the multidomain model performed better than the single-domain model. ΔAIC between the two models was ~100, indicating no empirical support for the single-domain model over its multidomain counterpart (Burnham & Anderson, 2003).

In terms of parsimony, the multidomain model has three input variables (precipitation rate, initial soil water content, and time) and as many as 15 parameters; the full set of parameters is listed in the Notation section. The single-domain Green-Ampt infiltration model has the same three input variables, but only up to seven additional parameters (roughly half as many as the multidomain model). Still, parameterization of the multidomain model was informed by physical measurements from soil samples and in situ infiltration measurements, along with fixed values for the crack partition coefficient ($\Upsilon = 0.75$), the shrinkage geometry factor ($\chi = 3$), and the Green-Ampt constant (A = 2/3). Noting that actual values of Υ and χ likely vary between soil types and moisture conditions (Chertkov et al., 2004; te Brake et al., 2013), these supplemental measurements and constraints allowed the Mexico site to be modeled with only three unknown parameters ($h_{f,\text{matrix}}$, $K_{\text{aggr,max}}$, and $K_{\text{interaggr,max}}$), and the Chile site to be modeled with only two unknown parameters ($K_{\text{interblock,max}}$, D_{soil}). Even though D_{soil} was treated as a semifitting factor for the Chile study (with two possible values used), in most instances its magnitude will be restricted over some narrow, plausible region (e.g., 0–3 m), thus limiting its ability to behave as a fully unconstrained parameter.

The multidomain model developed here has the ability to resolve four distinct pore domains: aggregates, interaggregate cracks (which together form the soil matrix), interblock border cracks, and subsidence. These domains all contribute to hydrological processes such as ponding, bypass flow, and overland flow, though certain domains only become relevant for certain scales and processes. For instance, the

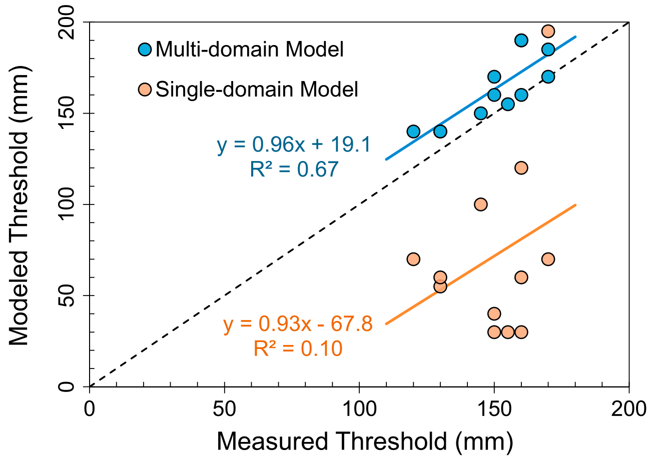

Figure 7. Measured thresholds, representing the amount of cumulative rainfall (mm) required for overland flow to begin in the 12 Chile runoff plots, versus simulated thresholds from the single-domain and multidomain models. The solid lines represent the linear trends; the dashed line indicates the 1:1 relationship.

interaggregate crack domain was necessary for simulating time to ponding and bypass flow in the Mexico study, where the scale of measurement focused on individual soil blocks. In the Chile study, where the scale of measurement focused on larger plot-level overland flow generation, the model showed negligible sensitivity to interaggregate cracks, as the combination of interblock crack and soil aggregate conductivities determined when the system transitioned from an infiltration- to runoff-dominated response. Nonetheless, including the interaggregate cracks helped to explain the variable infiltration rates within the soil matrix (Figure 3). Even though it comes at the cost of two extra parameters (Υ and $K_{\mathrm{interaggr,max}}$), the results here indicate that including both interaggregate and interblock cracks can facilitate simulations from the smaller soil matrix scale to the larger hillslope scale. Beyond the studies examined here, such differentiation of crack domains may also reconcile observed and modeled crack distributions, such as have been measured in laboratory (Chertkov & Ravina, 2002) and field settings (Bagnall, 2014; Neely et al., 2018).

Because it is based on the Green-Ampt approach, the model requires the assumptions that water moves as a piston through the cracks and that Darcy's law applies (i.e., Reynolds number $< \sim 10$). In reality, water often flows into cracks as films, a process that may be better represented using approaches such as the kinematic wave (Beven & Germann, 1981). Still, infiltration excess ponding within cracks likely occurs only in narrower cracks, where the above assumptions (piston flow with low Reynolds number) may apply. The model in its current form also does not allow for simulation of subsurface lateral flow, as was observed in both studies examined here and in other studies (e.g., Cammeraat, 2002). In this current work, such processes likely became lumped within the D_{soil} and hydraulic conductivity ($K_{\mathrm{interaggr,max}}$ or $K_{\mathrm{interblock,max}}$) terms. Still, bypass flow can be important for processes such as recharge (Kurtzman et al., 2016; Oostindie & Bronswijk, 1995) and solute transport (Bronswijk et al., 1995; van der Salm et al., 2012), meaning that future model developments should focus on describing downhill propagation of water flow through the shrinkage crack networks.

In conclusion, the model developed here better captures physical characteristics and hydraulic effects of shrinkage cracks and deformable soil matrices, while supporting the hypothesis that soil crack and matrix properties must be described separately to accurately simulate hydrological processes in shrink-swell soils. The model is parsimonious, for its equations do not require complex numerical schema to solve. Also, it is

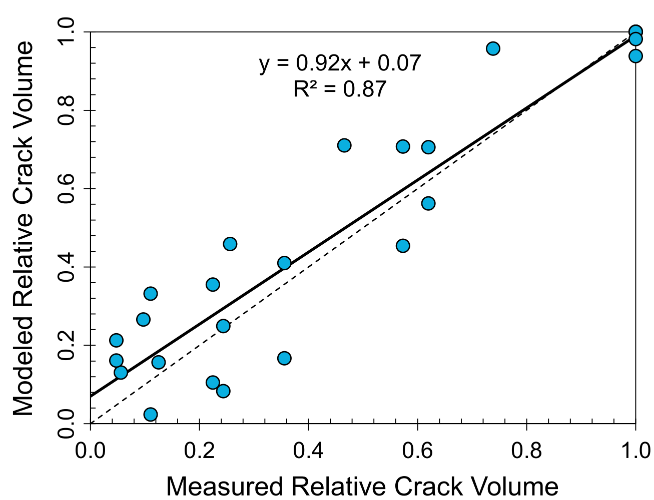

Figure 8. Measured versus modeled crack volumes in the Chile site, scaled relative to their maxima. Measured values came from five discrete cracks that were monitored during the rainfall-runoff experiments, while the modeled values were simulated by equation (4). The solid line represents the linear trend; the dashed line shows the 1:1 relationship.

10.1029/2018WR023297

possible with auxiliary measurements, such as infiltration tests and laboratory characterization of shrinkage and retention properties, to constrain (nearly) all of the required parameters. Still, relatively few previous studies have collected the types of data required to parameterize the model, providing an opportunity for future investigations to focus on and refine the parameters and processes revealed here as being important to the hydrology of shrink-swell soils.

Notation

Model Inputs

u_i	Initial gravimetric water content of the aggregate domain [−] (also normalized as U_i)
r	Rainfall rate [L T^{-1}]
t	Elapsed time [T]

Model Inputs

I	Total cumulative infiltration [L]
OF	Total cumulative surface runoff (overland flow) [L]
ΔU	Change in (normalized) water content [−]

Model Parameters (Note that * indicates parameters used in the single-domain model)

A	Constant used in the Green-Ampt solution (typically assumed to be 2/3)*
s	Depressional storage of the soil surface [L]*
$h_{f,\mathrm{matrix}}$	Wetting front potential of the soil matrix [L]*
D_{soil}	Depth of the *active* portion of the soil profile [L]*
D_{border}	Mean effective interblock (border) crack depth [L]
$u_{\max}$	Maximum (saturated) gravimetric water content [M M^{-1}]*
$\phi_{\max}$	Maximum point of the soil shrinkage curve (assumed as total soil porosity) [L^3 L^{-3}]*
$\phi_{\min}$	Minimum point of the soil shrinkage curve [L^3 L^{-3}]
$K_{\mathrm{aggr,max}}$	Maximum effective hydraulic conductivity of the aggregate domain [L T^{-1}]*
$K_{\mathrm{interblock,max}}$	Maximum effective hydraulic conductivity of the interblock crack domain [L T^{-1}]
$K_{\mathrm{interaggr,max}}$	Maximum effective hydraulic conductivity of the interaggregate crack domain [L T^{-1}]
Υ	Partition coefficient between interblock and interaggregate crack porosities ($0 \le \Upsilon \le 1$) [−]
χ	Shrinkage geometry factor ($\chi \ge 1$) [−]
p	Fitting parameter for the soil shrinkage curve [−]
q	Fitting parameter for the soil shrinkage curve [−]

Internal Model Parameters

$K_{\mathrm{matrix}}(U)$	Effective saturated hydraulic conductivity of the soil matrix [L T^{-1}]
$K_{\mathrm{border}}(U)$	Effective saturated hydraulic conductivity of the soil border cracks [L T^{-1}]
$\phi_{\mathrm{aggr}}(U)$	Aggregate porosity [L^3 L^{-3}]
$\phi_{\mathrm{crack}}(U)$	Total shrinkage crack porosity [L^3 L^{-3}]
$\phi_{\mathrm{interblock}}(U)$	Interblock (border) crack porosity [L^3 L^{-3}]
$\phi_{\mathrm{interaggr}}(U)$	Interaggregate crack porosity [L^3 L^{-3}]
$\phi_{\mathrm{sub}}(U)$	Subsidence porosity [L^3 L^{-3}]
n_e	Available pore space [L^3 L^{-3}]
$r_{\mathrm{matrix}}(U)$	Area-weighted rainfall rate on the soil matrix surface [L T^{-1}]
$r_{\mathrm{border}}(U)$	Area-weighted rainfall rate on the soil border cracks [L T^{-1}]
i_{matrix}	Infiltration rate into the soil matrix surface [L T^{-1}]
i_{border}	Infiltration rate into the soil border cracks [L T^{-1}]
$t_{p,\mathrm{matrix}}$	Time of ponding on the soil matrix surface [T]
I_{matrix}	Cumulative infiltration into the soil matrix surface [L]
$I_{p,\mathrm{matrix}}$	Cumulative infiltration into the soil matrix surface at time of ponding [L]
I_{border}	Cumulative infiltration into the soil border cracks [L]

Other Terms in Derivation

θ_s	Saturated volumetric water content [$L^3\ L^{-3}$]
θ_i	Initial volumetric water content [$L^3\ L^{-3}$]
ρ_s	Density of solid particles [$M\ L^{-3}$]
g	Gravitational acceleration constant [$L\ T^{-2}$]
μ_f	Dynamic viscosity of the fluid [$M\ L^{-1}\ T^{-1}$]
r_i	Radius of aggregate pore i [L]
$r_{i,\max}$	Maximum radius of aggregate pore i [L]
$r_{i,\min}$	Minimum radius of aggregate pore i [L]
l_j	Length of interblock crack j (assumed to be constant) [L]
w_j	Width of interblock crack j [L]
$w_{j,\max}$	Maximum width of interblock crack j [L]
y_k	Width of interaggregate crack k [L]
$y_{k,\max}$	Maximum width of interaggregate crack k [L]
A_k	Area of interaggregate crack k [L^2]
A_{total}	Total cross-sectional area of the soil [L^2]
$A_{\text{interblock}}$	Total cross-section area of all interblock cracks [L^2]
$A_{\text{interaggr}}$	Total cross-section area of all interaggregate cracks [L^2]
A_{aggr}	Total cross-sectional area of the aggregate domain [L^2]
$V_{\text{interblock}}$	Total volume of the interblock cracks [L^3]
$V_{\text{interaggr}}$	Total volume of the interaggregate cracks [L^3]
V_{aggr}	Total volume of the soil aggregate domain [L^3]
H_m	Height of the soil matrix [L]
τ_i	Tortuosity of aggregate pore i (assumed to be constant) [$L\ L^{-1}$]
τ_j	Tortuosity of interblock crack j (assumed to be constant) [$L\ L^{-1}$]
τ_k	Tortuosity of interaggregate crack k (assumed to be constant) [$L\ L^{-1}$]
M	Number of pores within the aggregate domain [−]
N	Number of cracks within the interblock crack domain [−]
O	Number of cracks within the interaggregate crack domain [−]
Q	Volumetric water flux through the soil (combined aggregate and crack domains) [$L^3\ T^{-1}$]
$Q_{\text{interblock}}$	Volumetric water flux through the interblock crack domain [$L^3\ T^{-1}$]
$Q_{\text{interaggr}}$	Volumetric water flux through the interaggregate crack domain [$L^3\ T^{-1}$]
Q_{aggr}	Volumetric water flux through the aggregate domain [$L^3\ T^{-1}$]
J	Darcian water flux through the soil (combined aggregate and crack domains) [$L\ T^{-1}$]
$J_{\text{interblock}}$	Darcian water flux through the interblock crack domain [$L\ T^{-1}$]
$J_{\text{interaggr}}$	Darcian water flux through the interaggregate crack domain [$L\ T^{-1}$]
J_{aggr}	Darcian water flux through the aggregate domain [$L\ T^{-1}$]
$\nabla\Psi$	Total gradient in potential driving water flow [$L\ L^{-1}$]
$\nabla\Psi_{\text{matrix}}$	Total gradient in potential driving water flow in the soil matrix [$L\ L^{-1}$]
$\nabla\Psi_{\text{border}}$	Total gradient in potential driving water flow in the interblock crack domain [$L\ L^{-1}$]
z	Depth of the wetting front in the Green-Ampt model [L]

Acknowledgments
Data from this paper are permanently archived at https://data.lib.vt.edu/files/sb397834q. Funding for this work was provided in part by the Virginia Agricultural Experiment Station and the Hatch Program of the National Institute of Food and Agriculture, U.S. Department of Agriculture.

References

Bagnall, D. K. (2014). Testing a mesopore and matrix model for use on shrink-swell soils. (M.S. Thesis), Texas A&M University, College Station, TX.

Beven, K., & Germann, P. (1981). Water flow in soil macropores. II. A combined flow model. *Journal of Soil Science*, *32*(1), 15–29. https://doi.org/10.1111/j.1365-2389.1981.tb01682.x

Bronswijk, J. (1988). Modeling of water-balance, cracking and subsidence of clay soils. *Journal of Hydrology*, *97*(3–4), 199–212. https://doi.org/10.1016/0022-1694(88)90115-1

Bronswijk, J. (1990). Shrinkage geometry of a heavy clay soil at various stresses. *Soil Science Society of America Journal*, *54*(5), 1500–1502. https://doi.org/10.2136/sssaj1990.03615995005400050048x

Bronswijk, J., Hamminga, W., & Oostindie, K. (1995). Field-scale solute transport in a heavy clay soil. *Water Resources Research*, *31*(3), 517–526. https://doi.org/10.1029/94WR02534

Burnham, K. P., & Anderson, D. R. (2003). *Model selection and multimodel inference: A practical information-theoretic approach*. New York, NY: Springer Science & Business Media.

Cammeraat, L. (2002). A review of two strongly contrasting geomorphological systems within the context of scale. *Earth Surface Processes and Landforms*, *27*(11), 1201–1222. https://doi.org/10.1002/esp.421

Chertkov, V. Y., & Ravina, I. (2002). Combined effect of interblock and interaggregate capillary cracks on the hydraulic conductivity of swelling clay soils. *Water Resources Research*, *38*(8), 1157. https://doi.org/10.1029/2000WR000094

Chertkov, V. Y., Ravina, I., & Zadoenko, V. (2004). An approach for estimating the shrinkage geometry factor at a moisture content. *Soil Science Society of America Journal*, *68*(6), 1807–1817. https://doi.org/10.2136/sssaj2004.1807

Coppola, A., Comegna, A., Dragonetti, G., Gerke, H. H., & Basile, A. (2015). Simulated preferential water flow and solute transport in shrinking soils. *Vadose Zone Journal*, *14*(9), 1–15. https://doi.org/10.2136/vzj2015.02.0021

Coppola, A., Gerke, H. H., Comegna, A., Basile, A., & Comegna, V. (2012). Dual-permeability model for flow in shrinking soil with dominant horizontal deformation. *Water Resources Research*, *48*, W08527. https://doi.org/10.1029/2011WR011376

Davidson, M. R. (1984). A Green-Ampt Model of infiltration in a cracked soil. *Water Resources Research*, *20*(11), 1685–1690. https://doi.org/10.1029/WR020i011p01685

Gérard-Marchant, P., Angulo-Jaramillo, R., Haverkamp, R., Vauclin, M., Groenevelt, P., & Elrick, D. (1997). Estimating the hydraulic conductivity of slowly permeable and swelling materials from single-ring experiments. *Water Resources Research*, *33*(6), 1375–1382. https://doi.org/10.1029/97WR00616

Greco, R. (2002). Preferential flow in macroporous swelling soil with internal catchment: Model development and applications. *Journal of Hydrology*, *269*(3-4), 150–168. https://doi.org/10.1016/S0022-1694(02)00215-9

Kurtzman, D., Baram, S., & Dahan, O. (2016). Soil–aquifer phenomena affecting groundwater under vertisols: A review. *Hydrology and Earth System Sciences*, *20*(1), 1–12. https://doi.org/10.5194/hess-20-1-2016

Lassabatère, L., Yilmax, D., Peyrard, X., Peyneau, P., Lenoir, T., Simunek, J., et al. (2014). New analytical model for cumulative infiltration into dual-permeability soils. *Vadose Zone Journal*, *13*(12), 1–15. https://doi.org/10.2136/vzj2013.10.0181

Morel-Seytoux, H. J., Meyer, P. D., Nachabe, M., Touma, J., van Genuchten, M. T., & Lenhard, R. J. (1996). Parameter equivalence for the Brooks-Corey and van Genuchten soil characteristics: Preserving the effective capillary drive. *Water Resources Research*, *32*(5), 1251–1258. https://doi.org/10.1029/96WR00069

Návar, J., Mendez, J., Bryan, R. B., & Kuhn, N. J. (2002). The contribution of shrinkage cracks to bypass flow during simulated and natural rainfall experiments in northeastern Mexico. *Canadian Journal of Soil Science*, *82*(1), 65–74. https://doi.org/10.4141/S00-047

Neely, H. L., Morgan, C. L. S., McInnes, K. J., & Molling, C. C. (2018). Modeling soil crack volume at the Pedon scale using available soil data. *Soil Science Society of America Journal*, *82*(4), 734–743. https://doi.org/10.2136/sssaj2018.01.0007

Novák, V., Šimůnek, J., & Van Genuchten, M. T. (2000). Infiltration of water into soil with cracks. *Journal of Irrigation and Drainage Engineering*, *126*(1), 41–47. https://doi.org/10.1061/(ASCE)0733-9437(2000)126:1(41)

Oostindie, K., & Bronswijk, J. (1995). Consequences of preferential flow in cracking clay soils for contamination-risk of shallow aquifers. *Journal of Environmental Management*, *43*(4), 359–373. https://doi.org/10.1016/S0301-4797(95)90266-X

Potkay, A. (2017). One-dimensional seepage in unsaturated, Expansive Soils. *Vadose Zone Journal*, *16*(11), 1–6. https://doi.org/10.2136/vzj2017.05.0105

Selker, J., & Assouline, S. (2017). An explicit, parsimonious, and accurate estimate for ponded infiltration into soils using the Green and Ampt Approach. *Water Resources Research*, *53*, 7481–7487. https://doi.org/10.1002/2017WR021020

Šimůnek, J., Jarvis, N. J., van Genuchten, M. T., & Gärdenäs, A. (2003). Review and comparison of models for describing non-equilibrium and preferential flow and transport in the vadose zone. *Journal of Hydrology*, *272*(1–4), 14–35. https://doi.org/10.1016/S0022-1694(02)00252-4

Stewart, R. D., & Abou Najm, M. R. (2018). A comprehensive model for single ring infiltration. 2: Estimating field-saturated hydraulic conductivity. *Soil Science Society of America Journal*, *82*(3), 558–567. https://doi.org/10.2136/sssaj2017.09.0314

Stewart, R. D., Abou Najm, M. R., Rupp, D. E., Lane, J. W., Uribe, H. C., Arumí, J. L., & Selker, J. S. (2015). Hillslope runoff thresholds with shrink-swell clay soils. *Hydrological Processes*, *29*(4), 557–571. https://doi.org/10.1002/hyp.10165

Stewart, R. D., Abou Najm, M. R., Rupp, D. E., & Selker, J. S. (2012). Measurement tool for dynamics of soil cracks. *Vadose Zone Journal*, *11*(2), 1–6. https://doi.org/10.2136/vzj2011.0048

Stewart, R. D., Abou Najm, M. R., Rupp, D. E., & Selker, J. S. (2014). Nondestructive quantification of macropore volume using shear-thinning fluid. *Soil Science Society of America Journal*, *78*(2), 445–453. https://doi.org/10.2136/sssaj2013.08.0346

Stewart, R. D., Abou Najm, M. R., Rupp, D. E., & Selker, J. S. (2016). Modeling multidomain hydraulic properties of shrink-swell soils. *Water Resources Research*, *52*(10), 7911–7930. https://doi.org/10.1002/2016WR019336

Stewart, R. D., Rupp, D. E., Abou Najm, M. R., & Selker, J. S. (2016). A unified model for soil shrinkage, subsidence, and cracking. *Vadose Zone Journal*, *15*(3), 1–15. https://doi.org/10.2136/vzj2015.11.0146

te Brake, B., van der Ploeg, M., & de Rooij, G. (2013). Water storage change estimation from in situ shrinkage measurements of clay soils. *Hydrology and Earth System Sciences*, *17*(5), 1933–1949. https://doi.org/10.5194/hess-17-1933-2013

van der Salm, C., van den Toorn, A., Chardon, W. J., & Koopmans, G. F. (2012). Water and nutrient transport on a heavy clay soil in a fluvial plain in the Netherlands. *Journal of Environmental Quality*, *41*(1), 229–241. https://doi.org/10.2134/jeq2011.0292

van Genuchten, M. T. (1980). A closed-form equation for predicting the hydraulic conductivity of unsaturated soils. *Soil Science Society of America Journal*, *44*(5), 892–898. https://doi.org/10.2136/sssaj1980.03615995004400050002x

Weiler, M. (2005). An infiltration model based on flow variability in macropores: Development, sensitivity analysis and applications. *Journal of Hydrology*, *310*(1–4), 294–315. https://doi.org/10.1016/j.jhydrol.2005.01.010